Cdk1 in germline and the dose of somatic EGFR signaling determine the rate of transit amplification

Purna Gadre[1], Shambhabi Chatterjee[1]*, Bhavna Varshney[1]*, Chetanchandra Joshi[1], Samir Gupta[1], Nitin Nitsure[2], and Krishanu Ray[1†]

[1]Department of Biological Sciences, and [2]School of Mathematics, Tata Institute of Fundamental Research, Colaba, Mumbai 400005, India

*- Contributed equally to the manuscript

† Correspondence: krishanu@tifr.res.in, krishanu64@gmail.com, Phone - +91-22-22782730, +91-22-22783919

Summary:

Stem cell progeny undergoes a series of mitoses, called transit amplifying (TA) divisions, before terminal differentiation. To quantify the impact of the intrinsic and extrinsic factors regulating the rates of TA divisions, we developed a simplified mathematical model which could predict the periods of the germline divisions from the stage-wise distributions of spermatogonial cysts in *Drosophila* testis. Analysis of the wild-type data using this model suggested that the cell cycle periods speed up after the second TA division due to shortening of the G1 phases. Further, suppression of the cell cycle checkpoint control in germline and upregulation of the somatic EGFR signaling is estimated to slow-down the rates of both the germline stem cell and TA divisions, increasing the cellular life spans at each stage. Together, these results suggest that higher levels of EGFR activation could attenuate cell division rates in the neighborhood, controlling the extents of tissue growth.

Running Head: Cdk1 and EGFR determine the TA rate

Keywords: EGFR, Spitz, Transit Amplification, germline stem cells, testis, *Drosophila*.

Highlights:

a) GSC progeny continues to divide at the same rate for two successive cycles.

b) Subsequent transition to transit-amplifying mode speeds up the proliferation rates.

c) Cdk1 expression in the germline cells controls the rates of GSC and TA divisions.

d) EGFR activation level in the somatic cyst cells determines the rate of TA divisions.

Introduction:

Adult stem cells often undergo an asymmetric division, producing a stem cell and a progenitor daughter. In many tissues, the stem cell progenitors further proliferate for several rounds, known as transit amplification (TA) divisions, before terminal differentiation (Rangel-huerta & Maldonado, 2017). Stem cells, which retain their mitotic potential for a long duration, are typically slow cycling cells, whereas their transit-amplifying daughters proliferate relatively rapidly and have a limited mitotic potential (Cotsarelis *et al*, 1990; Potten & Loeffler, 1990; Rangel-Huerta & Maldonado, 2017). Both the stem cell and TA cell proliferation is regulated by cell-intrinsic factors (Bowman *et al*, 2008; Weng *et al*, 2010; Mckearin & Spradling, 1990) and the microenvironment (Mandal *et al*, 2007; Festa *et al*, 2011; Xie *et al*, 2000; Vemaraju *et al*, 2012; (Doetsch *et al*, 2002) Kiger *et al*, 2000). Moreover, for both the cell types, the rates of cell divisions are altered in a similar fashion by hormonal stimulation (Giraddi *et al*, 2015), tissue damage (Lehrer *et al*, 1998; Ichijo *et al*, 2017), and aging (Charruyer *et al*, 2009). Defects in regulation of stem cell and TA divisions could lead to tumorigenesis (van der Flier & Clevers, 2009; Li *et al*, 2014; Janssens & Lee, 2014; Zhang & Hsu, 2017). Therefore estimating the rates of stem cell and TA divisions would be useful in investigating the mechanisms of tissue homeostasis. It could also help to model organ growth during development.

Drosophila testis is a well-characterized system to assess the impact of different cell intrinsic and extrinsic factors on the rates of GSC and TA divisions. The testis apex harbors ~10 germline stem cells (GSCs) and ~20 somatic cyst stem cells (CySCs). Asymmetric division of the GSCs produces the germline progenitor, gonialblasts (GBs), and that of CySCs produce the somatic cyst cells (SCCs). Each GB undergoes four rounds of symmetric TA divisions within an enclosure formed by two somatic cyst cells (SCCs), forming cysts containing 2, 4, 8 and 16 interconnected germline cells (Figure 1A). Subsequently, all the 16 germline cells within a cyst enter meiosis (Fuller, 1998). Comparative analysis of the data obtained from fixed tissue preparations suggested that the expression of the RNA-binding proteins - Held-Out-Wing (HOW) (Monk *et al*, 2010) and Bag-of-marbles (Bam) (Insco *et al,* 2009) in germ cells, and EGFR signaling in the neighboring somatic cells (Parrott *et al*, 2012) could antagonistically regulate the rates of GSC and TA divisions. The GSC division periods, estimated using the time-lapse imaging of intact testis preparations ex vivo, suggested that proportional distribution of symmetric and asymmetric rates of divisions are altered during regeneration (Sheng & Matunis, 2011). Also, periods of different cell cycle phases in GSCs are intrinsically regulated by the Rho/ROK signaling and AuroraB kinase (Lenhart & DiNardo, 2015). Together, this evidence indicates that the cell cycle rates are flexible and manages by a combination of factors in stem cells and at different stages of TA in *Drosophila* testis.

Adult stem cells and the TA systems in various tissues often adapt by establishing a new steady-state under different growth conditions influenced by environmental and physiological changes (Yang & Yamashita, 2015; Giraddi *et al*, 2015; Chiang *et al*, 2017; Lehrer *et al*, 1998). A recent report utilized dual labeling method using BrdU incorporation to estimate the rates of cell division at steady state in mouse neocortex (Harris *et al* 2018). It provided an indirect comparative estimate. Though this method appeared simple, BrdU incorporation has been shown to induce toxicity (Levkoff *et al*, 2008; Taupin, 2007), which might skew the results. The time-lapse imaging approach provides a direct measure of specific cell cycle intervals, but it is a tedious and time-consuming method for large-scale

screening of factors affecting the rates of TA divisions. In *Drosophila* testis, the GSCs are easily identifiable due to the characteristic floral arrangement around the hub, whereas the TA cysts are more abundant and tightly packed with no definite spatial marker for identification in live tissue (Figure 1B). Finally, germline cells in a cyst are interconnected by ring canals (Fuller, 1993), which allow the intercellular exchange of proteins (McLean & Cooley, 2013; Airoldi *et al*, 2011), making it difficult to distinguish the GSC clones from TA cyst clones using the clone-based methods (Luo, 2007; Evans *et al*, 2009). Therefore, mathematical modeling of the distribution obtained from fixed tissue data could offer an alternative estimate of the rates. Although multiple studies modeled dynamic changes in the stem cell behavior with varied conditions (Lei et al, 2014; Deasy et al, 2003; Hannezo *et al*, 2014), they were primarily focused on the stem cell behavior and required time-lapsed measurement of select parameters for experimental validation.

Here, we describe a simple mathematical formula that utilizes the demographics of GSCs and cysts at different stages to arrive at probabilistic predictions of their lifetimes at steady-state in the adult testis. Numerical solutions of the equations using the observed distribution of the live and dead cysts in fixed testis preparations suggested that halfway into the germline TA, the cell division periods are reduced by about 50% due to an intrinsic regulation. It also indicated that the suppression of cell cycle checkpoints in the germline, as well as prolonged somatic EGFR activation, either by ectopic sSpitz expression or due to the somatic knockdown of the known negative feedback regulators, argos (aos) and kekkon (kek1, and kek2), could slow down both the GSC and subsequent germline TA division periods. The loss of cell cycle checkpoint control in germline cells arrested the TA divisions and affected subsequent differentiation of the spermatogonial cysts. In contrast, constitutive EGFR activation in the SCCs at the later stages slowed down the TA and induced premature germ cell death. Altogether, these results suggest that cell cycle checkpoint control in the germline and EGFR signaling in the somatic neighborhood could define the rates of the germline divisions, and thereby, control the subsequent tissue growth and differentiation.

Results:

Mathematical analysis of stage-wise cyst distribution revealed a progressive reduction in the lifespans of germline cysts during the TA stages

The somatic and germline stem cells and the germline cysts are arranged in a radial order in wildtype testes (Figure 1B). With each division, cysts are displaced further away from the hub at the testis apex, and the cyst stage is identified by the number of germ cells in the tightly packed cluster (Figure 1C). Upon quantification of the number of cysts at each stage of the TA in wild-type testes, we found that the cyst numbers progressively reduce in successive TA stages (Figure 1D). In a closed system at steady state, the proportion of cells of a given stage would be equal to the proportional life-span of that stage if no cyst is lost due to death during the TA. We found that the relative distribution of cysts was invariant in the adult testis until 8-days after eclosion (Figure S1A), indicating that the rates of TA divisions remain in a steady state during this period. Consistent with a previous estimate (Yang & Yamashita, 2015), staining with Lysotracker, which marks the dying cells, and anti-Vasa marking the germline, also identified a few dead cysts at each TA stage (Figure S1B, C). To account for this observed germ cell death, we calculated the probability (s_i) of a

successful transition from one cyst stage to the next as a function of the the number of detected dead cysts (D_i) and the time of their persistence (A) in the tissue, termed as the clearance time. Assuming that the number of dying cysts at the transition from stage i to stage $i+1$ is D_i and expressing the quantity s_i in terms of the clearence time A and D_i we get the following equation.

$$T_{i+1} = \frac{N_{i+1}}{N_i}\left(\frac{T_i}{1 - D_i T_i / A N_i}\right) \quad (1)$$

In the above equation, N_i represents the observed average number of cysts at stage i, quantified from confocal images of isolated testes from different genetic backgrounds, and T_{i+1} and T_i are the lifetimes of stage $i+1$ and i respectively (supplemental method for a detail argument). The inclusion of the possibility of death in our model converts a simple linear succession of stages into a branched system, with a terminal branch at each vertex. Consequently, the simple linear ratios of numerical frequencies to periods used in a previous study for pupal ageing (Bainbridge & Bownes, 1981) now gets replaced by Möbius transformation. Such a transformation is non-linear, it leads to some unexpected behaviours near its singularity.

According to the time-lapse imaging analysis the average duration of a GSC division (T_0) is calculated as approximately 23.3 (Sheng & Matunis, 2011) and 14 hours (Lenhart & DiNardo, 2015), and the period of mitosis is reported as 40 minutes to 1 hour (Sheng & Matunis, 2011) and 30 minutes (Lenhart & DiNardo, 2015), respectively. The ratio between mitotic interval and the total division period multiplied by the average GSCs provides the GSC mitotic index. We used an average value of 50 minutes as the mitosis time to calculate the life span of GSCs from the mitotic indices estimated in different genetic backgrounds (Table 1, supplemental methods). The GSC lifespan estimate in the Canton-S matched the time reported by one (Sheng & Matunis, 2011), whereas the estimations in the *nanosGal4vp16 (nos>)* and *trafficjamGal4 (tj>)* backgrounds were in the range reported by the other study (Lenhart & DiNardo, 2015). These analyses indicated that the GSC time periods could vary considerably according to the genotypic background.

Germ cell death in *Drosophila* testis occurs in four sequential phases that are identified by the intensity and pattern of the Lysotracker staining (Chiang *et al*, 2017). Amongst these, phase-I to II transition is identifiable by an increase in the intensity of Lysotracker staining and the dye entry into the germ cell nucleus (Chiang *et al*, 2017 and figure S2). Therefore, we restricted the quantification of dead cysts to the Phase-I stage and "A" in Eq (1) is redefined as the Phase-I persistence time (Table S1). To estimate the average value of "A", we collected time-lapse images of Lysotracker stained testes, which revealed that all the TA stages exhibit large variation in the Phase-I duration (Table S2 and Figure S2). Furthermore, a limited simulation assuming the values of "A" as 0, 1, 2, 3, 4 and 5 hours indicated that the minimum clearance time during the I to IV cell stages should be at least 2 hours for a realistic prediction of the cyst division times in certain genetic backgrounds (Tables S3, for further explanation, refer to supplemental methods). We reasoned that a greater proportion in the death counts will be represented by the longer persisting dying cysts. Therefore, we assumed the value Phase-I duration as 4 hours for all stages of along with the estimated number of dead cysts at Phase-I at a given stage (D_i)

(Table S1) and the number of cysts in subsequent stages (Table S4). The value is consistent with the experimental data obtained from fixed tissue analysis (Chiang *et al*, 2017).

The predictions for the wild-type (Canton-S) background, grown at 25°C, indicated that the life spans of GBs (T_1, 1-cell stage, 30.8 hours) and the 2-cell stage (T_2, 29.8 hours) during the TA (Table 1) would be comparable to that of the average interval between successive divisions of a GSC (T_0 26.8 hours). In comparison, the life spans of the 4-cell (T_3, 13.1 hours) and 8-cell (T_4, 11.1 hours) stages are progressively shortened (Table 1). In other words, the GBs and germline cells in 2-cell stage divide at the same rate as GSCs whereas those in the 4 and 8-cell cysts divide at ~50% faster rates.

The genetic background controls, *viz.*, *nos>EGFP* and *tj>HisRFP* were grown at 29°C for 4 days post adult eclosion for optimum Gal4 mediated expression. The lifespan calculations of TA stages in the *nos>EGFP* background yielded values comparable to the Canton-S control (Table 1). However, unlike the Canton-S, the GSC lifespans in the *nos>EGFP* testes was predicted be significantly shorter at 14.8 hours, which is consistent with nearly 2-fold higher mitotic index and a comparatively lower number of GSCs found in these specimen (Table S4 and S5), and similar to the values reported by Lenhart & DiNardo, 2015 earlier. The estimations in the *tjGal4>HisRFP* background yielded substantially shorter life-spans of all stages including the GSCs as compared to other controls. In all these backgrounds, there was a consistent ~50% reduction in the lifespans of the 4-cell stage from that of the 2-cell stage. These differences indicate the mitotic indices and the frequency of germ cell deaths determined the distribution of the germline cysts in different genetic backgrounds. It also indicated that a steady state is achieved by a combination of multiple stem cell and TA cell behaviors.

To understand the correlation between the rates of TA divisions and that of the cell cycle phases, we scored the frequency of different cell cycle markers spanning the G1 phase to M phase in wild-type testes. It suggested that except for the G_1 phases the S, G_2, and M-phases persist for similar durations during each TA division (Figure 1C, D). The duration of G_1 phases, however, as highlighted by the proportion of Cyclin E-positive cysts significantly declined after the 2-cell stage. Cyclin E level peaks at the G_1/S transition (Bertoli *et al*, 2015). Therefore, the length of the G1-S transition phase is likely to shrink proportionately with that of the cell division periods during the TA. In addition, we also noted that the sum of the proportion of cysts marked by the cell cycle phase markers in the GB and 2-cell stages were less than the total cysts found at those stages (Figure S1D). It suggests that both the GB and 2-cell stage spermatogonial cells could go through a quiescence phase in between the cell cycles.

Loss of cell cycle checkpoint control slowed down the rates of germ cell divisions.

To verify the mathematical formulation (Eq-1), we sought to deliberately alter the TA division rates by knocking down Cdc25/String and Cdk1, and overexpressing *Drosophila* p53 in the germline, and calculate the effects. Inhibition of Cdk1, a conserved cell cycle checkpoint protein, attenuates entry into the M phase (Nurse, 1990). Also, the loss of *string* (*stg*), which codes for a Cdc25 phosphatase required to remove the inhibitory phosphorylation on Cdk1 facilitating the G_2-M transition (Zielke *et al*, 2014; Bouldin & Kimelman, 2014), is reported to reduce the mitotic potential of GSCs in *Drosophila* testis (Inaba *et al*, 2011). We found that the *stg* and *Cdk1* RNAi reduced the frequency of GSC

divisions (Table S4) as well as the cysts number at subsequent stages (Figure 2B, C, and E). The dp53 protein is involved in arresting cell division or inducing death in response to cellular stress such as DNA damage, tumorigenesis, and starvation at the G1 and G2 checkpoints (Levine, 1997; Chen, 2016). The overexpression of dp53 reduced the cyst counts (Figure 2 D-E). Also, the GSC mitotic indices (Table S4) and the average number of mitotically active cysts at early stages, marked by phospho-Histone 3 (PH3) immunostaining (Figure 2F), were significantly reduced. Together, these observations suggested that alteration of cell cycle controls in the early germline could alter the cyst distribution profiles in adult testis.

The cyst distribution in the *nos>stg*^{dsRNA} and *nos>dp53* backgrounds remained invariant until 8 days after eclosion at 29°C and calculations using Eq-1 suggested at least 2-fold slowdown of the GSC division rates in all three cases as compared to the control (Table 2). The effects of *stg* and *Cdk1* RNAi was restricted to only the GSC divisions. Since stg is only expressed in the GSCs (Inaba *et al*, 2011), it explained the effect being limited to this stage. The results in *Cdk1* RNAi background may indicate an insufficient level of the *nosGal4>Cdk1*^{dsRNA} expression in the TA stages. In comparison, the dp53 overexpression is indicated to strongly suppress both the GSC and subsequent TA division rates (Table 2).

To understand their role during the later stages, we expressed the *stg*^{dsRNA}, *Cdk1*^{dsRNA} (Figure 3) and *dp53* transgenes (Figure S3) using the *bamGal4*. Cdc25/string has been shown to be selectively expressed in the GSCs (Inaba *et al*, 2011). Hence, the expression of *stg*^{dsRNA} transgene in 4-16 cell cysts did not alter the cyst distributions (Figure 3A). In the *bam>Cdk1*^{dsRNA} testes, the numbers of GSCs, GBs, and 2-cell cysts were similar to that of the control, the number of 4-cell cysts was significantly higher, and the testes were filled with 8-cell cysts (Figure 3B). Consistent with the previous results, these data further suggested that Cdk1 plays a critical role in TA progression and its partial loss could attenuate the rates of TA divisions. The *bamGal4>dp53* overexpression caused widespread germ cell death (Figure S3A, arrows). Often we noticed cysts with >32 germ cells within a cyst (Figure S3A, arrowhead) with compact chromatin morphology similar to that of the spermatogonia (Figure S3Bb, arrowhead). Due to punctate and irregular armadillo staining (Figure S3A), we could not estimate the cyst distribution profile in these testes however the GSC counts were not significantly different than that of the control (Figure S3C). These results indicated that dp53 overexpression in the germline at late TA stages could be detrimental to meiotic entry and progression. Together these results emphasized the effectiveness of the model in extracting the underlying differences in the rates of GSC and TA divisions which were not often apparent from the cyst distribution profiles.

Elevated levels of somatic EGFR activation did not promote a premature germline differentiation

The proliferating germ cells secrete an EGF ligand, Spitz, which activates the EGFR signaling in the encapsulating SCCs. The EGFR-ERK signaling is suggested to be the key regulator of the TA (Gupta *et al*, 2018). Additionally, it has been shown that loss of EGFR signaling in the somatic cells increases the mitotic indices of the GSCs (Parrott *et al*, 2012), and leads to the uncontrolled proliferation of undifferentiated germline cells within a cyst (Kiger *et al*, 2000). The somatic EGFR activation is implicated in maintaining synchronous, germ cell divisions within a cyst (Gupta *et al*, 2018). Moreover, an excessive EGFR signaling

is proposed to advance the germline differentiation by inducing a premature meiotic transition (Hudson *et al*, 2013). Therefore, to understand the role of EGFR signaling during the TA, we investigated the effects of EGFR gain of function on the GSC and TA stages.

Ectopic induction of a constitutive active (CA) form of the human EGFR ($EGFR^{CA}$) in SCCs using the *tjGal4 tub-gal80^{ts}* system (Figure 4B, C) progressively reduced both the GSCs and germ cell population (Table S6A, Figure 4C). EGFR antibody staining in these testes reported that the transgene continued to express until the early spermatocyte stage beyond the TA stages (Figure. S4A). Upon enumeration of the stage-specific distribution we found that after 96 hours (4-days) of *$EGFR^{CA}$* overexpression, the GB population decreased marginally whereas that of the 2-, 4-, and 8-cell cysts declined significantly (Figure 4D-b). Some of these cysts carried abnormally large germ cells (arrowhead, Figure S4A, and S5B) and we also observed SCCs with enlarged cytoplasm (arrows, Figure S5B-f, and C-b). Lysotracker staining indicated a substantial increase in the germ cell death at 24 hours (Figure 4E). We also noted a visible increase in the number of dead cysts from 18 hours (Figure 4E-b) with the nuclear diameters of the dying cells matching that of the S3 stage spermatocytes Figures S4C, D, and S5B) indicating that the germ cell death in the EGFR gain of function background, is perhaps induced in cysts after the completion of TA. A similar conclusion was obtained by a recent study (Papagiannouli *et al*, 2018). Since *tj>$EGFR^{CA}$* expression in SCCs persisted beyond the TA stages (Figure S4A), we concluded that persistent high dose of somatic EGFR signaling during the late TA is detrimental for the viability of the germline cells.

The somatic over-activation of EGFR downstream is reported to induce premature germline differentiation generating less than 16 cell spermatocyte cysts (Hudson *et al.*, 2013). However, the stagewise enumeration data presented here failed to support this argument. We did not find an anomalous increase in the proportions of early-stage cysts after increasing $EGFR^{CA}$ levels in the SCCs for four days. Also, a majority of the germ cell death was observed in the meiotic cysts. Hence, we concluded that instead of early induction of meiosis, the activation of the somatic EGFR signaling could slowdown germ cell division within a cyst leading to premature death during the early spermatocyte stage.

Increased ligand (Spitz) secretion from the germline slowed down the rates of germline TA divisions

A relatively milder, EGF overexpression paradigm using the *nos>sSpi-GFP* stock with visible sSpi-GFP expression in the GSCs and GBs (Figure 5A-a,b) helped to establish a new steady state during the adult stages with a significantly reduced number of cysts at all stages (Figure 5B). The number of GBs and 2-cell cysts marked by the PH3 staining was also significantly reduced (Figure 5C). We noticed an increase in the average number of dead GBs (Table S1B), but there was no abnormal germ cell death at the spermatocyte stage in this background. Time-lapse imaging of *nos>sSpi-GFP* testes stained with the Lysotracker suggested that the Phase-I durations in this background were within the wild-type range (Table S2B). Computing these enumerations with Eq-1 predicted a slowdown of the GSC and the subsequent TA divisions by ~2-fold as compared to the control (Table 3). This analysis suggested that persistent or increased somatic EGFR signaling could reduce the rates of neighboring GSC and GB divisions which could induce a slowdown in the subsequent TA stages. However, we also noted that the *nos>EGFP* expression marked

almost the entire TA (Figure 5A-c), suggesting that comparatively lower levels of sSpi-GFP could persist during the later stages of the TA.

Therefore, to characterize the role of EGFR signalling in the later stages, we overexpressed the *sSpiGFP* transgene using the *bamGal4*, which enlarged the cytoplasm of somatic cyst cells surrounding the 4 to 16-cell cysts (arrowheads, Figure 5D-a) and significantly increased the populations of 4, 8, and 16-cell cysts (Figure 5D). The latter observation confirmed a significant slowdown in the TA rates. Together, these results established that ectopic increase in the somatic EGFR signaling slows down the germline divisions and subsequent differentiation.

Loss of the EGFR feedback inhibition in SCC also slowed the rates of germline divisions

The EGFR downstream cascade activates three different feedback inhibitors (Figure 6A), *argos* (*aos*) *kekkon* (*kek*), and *sprouty* (*spry*) (Ghiglione *et al*., 1999; Reich *et al.*, 1999; Golembo *et al*., 1996). Analysis of the GFP pattern in testes obtained from the *aos-GFP* ^{fTRG} fosmid (Figure 6B), the *kek1-GFP* promoter-trap (Figure 6C) transgenic backgrounds suggested that both the genes are expressed in SCCs during the early stages. The *aos-GFP* expression was comparatively weaker and localized around the GSCs, and germline cells in the TA region (Figure 6B). Expression of the *kek1-GFP* promoter trap marked the nuclei of SCCs in the TA region and beyond (Figure 6C). Since GFP is relatively more persistent than the fusion proteins, we could only interpret the onset of the *kek1* promoter expression from this transgene.

To understand the effect of the moderate gain of somatic EGFR signaling on the TA divisions, we estimated the stage-specific distribution of cyst populations in *aos*, *kek1,* and *kek2* RNAi backgrounds. All the three conditions reduced the number of GSCs and 1-cell cysts (Figure 6D-I). *kek1* RNAi also reduced the population of 2-cell cysts (Figure 6E, F). In addition, the average mitotic indices of GSCs were reduced in the *aos* and *kek2* RNAi backgrounds (Table S4), suggesting a slowdown of the GSC divisions. There was an overall decrease in the average number of mitotically active cysts in all the RNAi backgrounds as compared to control (Figure 6G). The stage-specific lifespan calculations using Eq-1 predicted nearly 2-fold slowdown at each stage in the *aos* and *kek2* RNAi backgrounds (Table 4). The effect was most pronounced in the *kek2* RNAi background. We could not calculate the TA periods in *kek1* RNAi backgrounds due to the absence of PH3-stained GSC in the observed cohort (Figure 6G). Thus, Kekkon-mediated negative feedback appeared to play a more significant role as compared to Argos in moderating the EGFR signaling in testis. Together with the *sSpi-GFP* overexpression data, these results indicated that the extension or increased levels of EGFR activation in SCCs could attenuate the rates of TA divisions at all stages.

Discussion:

Germline cells transitions to transit amplifying mode after the onset of bam expression

Adult stem cells are maintained in a quiescent phase (G_0) for extended durations with occasional induction of cell cycle phase whereas transit amplifying cells cycle rapidly without the intervening G_0 phase (Cheung & Rando, 2013; Lajtha, 1979). We found that the total proportion of GBs and 2-cell cysts marked by different cell-cycle phase reporters are less than the total number of cysts at these two stages. In comparison, the proportion of cysts undergoing active cell-cycle in 4 and 8-cell stages are similar to the total cysts. The analysis of GSC and stage-specific cyst distribution also indicated that GSCs, 1- and 2-cell cysts divide at a comparable rate whereas the germline cells in the 4 and 8-cell cysts divide at a progressively faster rate. The predictions indicated a bimodal distribution with the lifespans of early stages (GB and 2-cell) comparable to that of GSCs, and those of the subsequent stages (4 and 8-cell) appeared to be 2-fold shorter. Therefore, similar to GSCs, the GBs and spermatogonial cells in 2-cell cysts could go through a G_0 phase between active cell divisions indicating a change in the pattern of cell division before and after the onset of bam expression in the testis.

In line with a previous report (Inaba *et al*, 2011), we found that the String function is only important in the stem cells. Earlier studies have reported that temperature-sensitive mutants of *cdc2* (Cdk1) are only defective in meiotic progression during *Drosophila* spermatogenesis and Twine is implicated in Cdk1 activation (Sigrist *et al*, 1995). In this study, we showed that Cdk1 is also essential for the TA progression in 4 and 8-cell stages. These results suggested a role of Cdk1 and G2-M checkpoint regulation in the stem cells and during TA stages. The *dp53* gene is expressed in the spermatogonial stages (Napoletano *et al*, 2017). It is also activated in response to radiation-induced DNA damage (Wylie *et al*, 2014). Overexpression of *dp53* induces necrosis, and its absence leads to hyperplasia (Napoletano *et al*, 2017). We showed that *dp53* overexpression in the late stages of the TA induced cell death and blocked entry into meiosis. Together these results suggest that p53 activity and expression might be inhibited in primary spermatocytes to facilitate entry into meiosis.

Remodeling of cell cycle rates at the 4/8-cell stage of the germline TA was also reported in the *Drosophila* ovary (Hinnant *et al*, 2017). Incidentally, this transition coincides with the onset of bam expression at this stage (Insco *et al*, 2009). The Bam threshold has already been shown to play a critical role in arresting the TA before the meiotic transition (Insco *et al,* 2009). These observations further suggested that the onset of Bam could play a role in remodeling the cell cycle from the stem-like divisions to fast amplifying TA division at the 4-cell stage.

Somatic levels of EGFR signaling independently controls the rates of GSC and TA divisions

The rate of adult stem cell division affects the rate of production of differentiated progeny. A reduction in the rate of GSC divisions with aging in *Drosophila* ovary slows down the egg production rate (Zhao *et al*, 2008). Similarly, the GSC mitotic index declines in *Drosophila* testis with aging owing to depletion of String from the GSCs (Inaba *et al*, 2011) and we found that GSCs divide even more slowly in the *stg* and *Cdk1* RNAi backgrounds. The mathematical modeling of the experimental data further predicted that along with the downregulation of cell cycle checkpoint proteins in the germline, the upregulation of EGFR signaling in the neighboring somatic cells could attenuate the rate of GSC divisions. The

sSpi-GFP overexpression in GSCs and early germline cells, as well as the loss of aos and kek-2 from the somatic cells, reduced the GSC mitotic index indicating a significant reduction in the division rate. It also prolonged the cell cycle periods in subsequent TA stages reversing the trend at the 4-cell stage. The loss of EGFR signaling increased the rates of GSC and germline TA divisions within a cyst and arrested differentiation (Kiger *et al*, 2000; Parrott *et al*, 2012; Gupta *et al*, 2018). The upregulation EGFR, on the other hand, is found to slow down the GSC and TA proliferation rates without affecting differentiation. Therefore, the dose of the EGFR signaling is likely to play a critical role in determining the rates of cell divisions in the neighborhood.

The premature arrest of the TA divisions at the 8-cell stage in the *bam>Cdk1*^{dsRNA} background affected the subsequent induction of meiosis. It may indicate that the timely progression of cell division is essential for tissue differentiation. The slowdown of TA divisions due to increased EGFR signaling in the early stages did not appear to affect spermatocyte differentiation. However, the EGFR^{CA} overexpression in SCCs led to spermatocyte death indicating that the extension of EGFR signaling beyond the TA stages is detrimental to the differentiation and survival of germ cells. Recent studies have reported that upregulation of EGFR signaling induces apoptotic death in cancer cell lines (Choi *et al*, 2010; Högnason *et al*, 2001; Treda *et al*, 2016; Kim *et al*, 2015) and on the whole-organism level in *C. elegans* (Jiang & Wu, 2014). These observations may suggest that appropriate tuning of the EGFR signaling dose is important for maintaining a balance between survival and death during the TA.

Mathematical modeling of tissue growth in *Drosophila* testis and other germline systems

Tissues adapt to the environmental changes such as nutrient depletion, hormonal stimulation, wound healing, *etc*. and transition between different states of homeostasis (Yang & Yamashita, 2015; Giraddi *et al*, 2015; Chiang *et al*, 2017; Lehrer *et al*, 1998). The quantitative data interpretation in this area has been limited to the stem cells (Roth *et al*, 2012; Rodgers *et al*, 2014; Seidel & Kimble, 2015; Cotsarelis *et al*, 1990; Inaba *et al*, 2011; Ojeh *et al*, 2015). Often the transit amplifying pool was considered as homogenous proliferative population. The gene expression analysis in *Drosophila* ovary and testis, however, indicated a certain degree of genetic differentiation during the TA (Insco *et al*, 2009; Li *et al*, 2009). Clonal segregation of germline in the somatic encapsulated cysts in this tissue further helped to discriminate and enumerate the stage-specific distribution in the adult testis in this study. We have utilized this property to formulate a lifetime prediction method which provided a rich understating of TA regulation by somatic EGFR signaling in *Drosophila* testis. This model allowed us to calculate the lifespans of different cell types within the tissue by enumerating the steady-state distribution in fixed preparations. It demonstrated that one could estimate the average lifetimes of different demographic stages in a steady state system using simple data such as the progeny number, cell death, and mitotic index.

This method can be easily used to obtain quantitative distinctions of the TA rates in the germline in different genetic backgrounds and those altered by environmental perturbations. One of the limitations of this method is the requirement of stage-wise discrimination of cellular lineage to identify cells at different stages of transit amplification within a tissue. We envisage that one could adapt the formula by careful calibration of the dye tracing data in the progeny of other stem cells such as the type II neuroblasts in

Drosophila (Boone & Doe, 2008)(Homem & Knoblich, 2012), skin epidermal stem cells in *Zebrafish* (Guzman *et al*, 2013), mouse corneal epithelial stem cells (Kawasaki *et al*, 2006), and mammalian intestinal stem cells (van der Flier & Clevers, 2009) in the future.

Materials and methods

Drosophila stocks and culture condition

All stocks and crosses were maintained on standard *Drosophila* medium at 25°C unless mentioned otherwise. The flies were reared for four days at 29°C before dissection and fixation as described before (Joti *et al*, 2011). A detailed stock list is mentioned in Table S9.

EGFR-time course experiments

The crosses were reared at 18°C. Freshly eclosed adult males were shifted to 30°C for mentioned periods. For recovery experiments, the crosses were reared at 18°C, and the adult males were heat-shocked at 30°C for 24 hours. Subsequently, the males were shifted back to 18°C for the mentioned periods.

Whole-mount immunofluorescence-staining

Testes from a four-day-old male were dissected in Phosphate buffer-saline (PBS) and fixed in 4% paraformaldehyde for 20 to 30 minutes at room temperature. The testes were then washed 3 times in PTX (0.3% Triton-X100 in PBS). Incubated in blocking solution PBTX (5% BSA in PTX) and incubated with an appropriate dilution of primary antibodies in for overnight. Samples were washed 3 times in PTX followed by a 2-hour incubation at room temperature with Alexa dye-conjugated secondary antibodies Invitrogen) at 1:200 dilution in PBTX, and a final set of wash in PTX. The samples were mounted with a drop of Vectashield® (Vector Laboratory Inc., USA). For visualizing the nucleus, the samples were incubated with 0.001% Hoechst-33342 (Sigma Chemical Co. USA) for 20 minutes post the entire immunostaining protocol. Then the samples were washed with PTX and mounted as mentioned above. The following primary antibodies were used: rat anti-Vasa (1:50; Developmental Studies Hybridoma Bank (DSHB); developed by A. Spradling, Carnegie Institution for Science, USA), mouse anti-Armadillo (1:100; DSHB; E. Wieschaus, Princeton University, USA), rabbit anti- phospho-Histone-3 (1:4000, Santa Cruz Biotechnology); anti-EGFR (Gift from Ben-Zion Shilo), mouse anti-cyclin A (DSHB, C.F. Lehner, University of Bayreuth, Germany), rabbit cyclin-E (1:100, Santa Cruz Biotechnology).

Determination of GSC mitotic index

PH3 positive GSCs were quantified in different genetic backgrounds (table 1). The GSC mitotic index was quantified by dividing the total number of PH3 positive GSCs by the total number of GSCs in that particular genotype. The calculations used to determine GSC cycling time have been described in the supplemental method, section 13 and 14.

Quantification of germline cell death (GCD)

For detection of GCD, testes were stained with Lysotracker RedDND-99 (Life Technologies) in PBS for 30 min before paraformaldehyde fixation. For further details refer to a supplemental method, section 11, and the data is presented in Table S1.

Image acquisition, analysis, and cyst profile quantification

Images were acquired using Olympus FV1000SPD laser scanning confocal microscope using 10X, 0.3 NA and 60X, 1.35 NA or Olympus FV3000SPD laser scanning confocal microscope using 60X, 1.42 NA objectives or Zeiss 510meta laser scanning confocal microscope using the 63X, 1.4 NA objective. Multiple optical slices were collected covering the entire apical part of the testes. The images were analyzed using ImageJ® (http://fiji.sc/Fiji). The Cell-counter™ plugin was used for quantification of the immunostained cysts. The Origin (OriginLab, Northampton, MA) software and Microsoft Excel (2013) was used for all statistical analysis. A detailed derivation of the mathematical model is presented in supplemental methods.

Acknowledgment

We thank Benny Shilo, Talila Volk and Eli Arama, Weismann Institute, Israel; Kenneth Irvine, Waksman Institute of Microbiology, New Jersey, USA; Dorothea Godt, Univ. Toronto, Canada; Lynn Cooley, Yale School of Medicine, Connecticut, USA; Dennis McKearin, Bloomington Stock Center, Indiana, USA; Vienna Drosophila Resource Center, Austria; and Developmental Studies Hybridoma Bank, Iowa, USA; for fly stocks and other reagents. A special thanks to Prof. Shilo for critical comments and suggestions.

Author's contribution

P.G., and S.C., B.V., C.J., and S.G., performed experiments. P. G., S. C., and K.R. analyzed the data. N.N. P.G. K.R. and S.G. developed the mathematical theory. P.G. and K.R. composed the figures and drafted the manuscript. All the authors contributed equally in evolving the concept.

Competing interests

The authors have no competing interest in the publication of the results.

Funding

K.R., P.G., B.V., and S.G. were supported by an intramural fund of TIFR, Dept. of Atomic Energy (DAE), Government of India. S.C., and C.J. were supported by the Department of Biotechnology (DBT), Government of India. The study was partly supported by the DBT grant BT/PR/4585/Med/31/155/2012 (dated 28 September 2012) and in part by the intramural funding of TIFR, DAE.

References:

Airoldi SJ, McLean PF, Shimada Y & Cooley L (2011) Intercellular protein movement in syncytial Drosophila follicle cells. J. Cell Sci. 124: 4077–4086

Bainbridge SP & Bownes M (1981) Staging the metamorphosis of Drosophila melanogaster. J. Embryol. Exp. Morphol. 66: 57–80

Bertoli C, Skotheim JM, Bruin RAM De, Street G & de Bruin RAM (2015) HHS Public Access. Nat. Rev. Mol. Cell Biol. 14: 518–528

Boone JQ & Doe CQ (2008) Identification of Drosophila type II neuroblast lineages containing transit amplifying ganglion mother cells. Dev. Neurobiol. 68: 1185–1195

Bouldin CM & Kimelman D (2014) Cdc25 and the importance of G2 control Insights from developmental biology. Cell Cycle 13:14, 2165–2171

Bowman SK, Rolland V, Betschinger J, Kinsey KA, Emery G & Knoblich (JA 2008) The Tumor Suppressors Brat and Numb Regulate Transit-Amplifying Neuroblast Lineages in Drosophila. Dev Cell. 14(4): 535–546.

Charruyer A, Barland CO, Yue L, Wessendorf HB, Lu Y, Lawrence HJ, Mancianti ML & Ghadially R (2009) Transit-amplifying cell frequency and cell cycle kinetics are altered in aged epidermis. J. Invest. Dermatol. 129: 2574–2583

Chen J (2016) The Cell-Cycle Arrest and Apoptotic and Progression. Cold Spring Harb. Perspect. Med. 6: 1–16

Cheung TH & Rando TA (2013) Molecular regulation of stem cell quiescence. Nat. Rev. Mol. Cell Biol. 14: 329–340

Chiang AC-Y, Yang H & Yamashita YM (2017) spict, a cyst cell-specific gene, regulates starvation-induced spermatogonial cell death in the Drosophila testis. Sci. Rep. 7: 40245

Choi J, Moon SY, Hong JP, Song J, Oh KT & Lee S (2010) Epidermal Growth Factor Induces Cell Death in the Absence of Overexpressed Epidermal Growth Factor Receptor and ErbB2 in Various Human Cancer Cell Lines. Cancer Invest. 28: 505–514

Cotsarelis G, Sun TT & Lavker RM (1990) Label-retaining cells reside in the bulge area of pilosebaceous unit: Implications for follicular stem cells, hair cycle, and skin carcinogenesis. Cell 61: 1329–1337

DasGupta R & Fuchs E (1999) Multiple roles for activated LEF/TCF transcription complexes during hair follicle development and differentiation. Development 126: 4557–68

Evans CJ, Olson JM, Ngo KT, Kim E, Lee NE, Kuoy E, Patananan AN, Sitz D, Tran PT, Do MT, Yackle K, Cespedes A, Hartenstein V, Call GB & Banerjee U (2009) G-TRACE: Rapid Gal4-based cell lineage analysis in Drosophila. Nat. Methods 6: 603–605

Festa E, Fretz J, Berry R, Schmidt B, Rodeheffer M, Horowitz M & Horsley V (2011) Adipocyte Lineage Cells Contribute to the Skin Stem Cell Niche to Drive Hair Cycling. Cell 146: 761–771

van der Flier LG & Clevers H (2009) Stem Cells, Self-Renewal, and Differentiation in the Intestinal Epithelium. Annu. Rev. Physiol. 71: 241–260

Fuller MT (1998) Genetic control of cell proliferation and differentiation in Drosophila spermatogenesis. Semin. Cell Dev. Biol. 9: 433–44

Ghiglione C, Carraway KL, Amundadottir LT, Boswell RE, Perrimon N & Duffy JB (1999) The Transmembrane Molecule Kekkon 1 Acts in a Feedback Loop to Negatively Regulate the Activity of the Drosophila EGF Receptor during Oogenesis. Cell 96: 847–856

Giraddi RR, Shehata M, Gallardo M, Blasco MA, Simons BD & Stingl J (2015) Stem and progenitor cell division kinetics during postnatal mouse mammary gland development. Nat. Commun. 6: 1–12

Golembo M, Schweitzer R, Freeman M & Shilo BZ (1996) Argos transcription is induced by the Drosophila EGF receptor pathway to form an inhibitory feedback loop. Development 122:

Gupta S, Varshney B, Chatterjee S & Ray K (2018) Somatic ERK activation during transit amplification is essential for maintaining the synchrony of germline divisions in Drosophila testis. Open Biol. 8: 180033.

Guzman A, Ramos-Balderas JL, Carrillo-Rosas S & Maldonado E (2013) A stem cell proliferation burst forms new layers of P63 expressing suprabasal cells during zebrafish postembryonic epidermal development. Biol. Open 2: 1179–1186

Hannezo E, Prost J & Joanny JF (2014) Growth, homeostatic regulation and stem cell dynamics in tissues. . R. Soc. Interface 11: 20130895.

Harris L, Zalucki O & Piper M (2018) Correction to: BrdU/EdU dual labeling to determine the cell-cycle dynamics of defined cellular subpopulations. J. Mol. Histol. 49: 447

Hinnant TD, Alvarez AA & Ables ET (2017) Temporal remodeling of the cell cycle accompanies differentiation in the Drosophila germline. Dev. Biol. 429: 118–131

Högnason T, Chatterjee S, Vartanian T, Ratan RR, Ernewein KM & Habib AA (2001) Epidermal growth factor receptor induced apoptosis: Potentiation by inhibition of Ras signaling. FEBS Lett. 491: 9–15

Homem CCF & Knoblich JA (2012) Drosophila neuroblasts: a model for stem cell biology. Development 139: 4297–4310

Hudson AG, Parrott BB, Qian Y & Schulz C (2013) A Temporal Signature of Epidermal Growth Factor Signaling Regulates the Differentiation of Germline Cells in Testes of Drosophila melanogaster. PLoS ONE 8(8): e70678

Ichijo R, Kobayashi H, Yoneda S, Iizuka Y, Kubo H, Matsumura S, Kitano S, Miyachi H, Honda T & Toyoshima F (2017) Tbx3-dependent amplifying stem cell progeny drives interfollicular epidermal expansion during pregnancy and regeneration. Nat. Commun. 8: 1–12

Inaba M, Yuan H & Yamashita YM (2011) String (Cdc25) regulates stem cell maintenance, proliferation and aging in Drosophila testis. Development 138: 5079–5086

Insco ML, Leon A, Tam CH, McKearin DM & Fuller MT (2009) Accumulation of a differentiation regulator specifies transit amplifying division number in an adult stem cell lineage. Proc. Natl. Acad. Sci. 106 (52) 22311-22316

Janssens DH & Lee CY (2014) It takes two to tango, a dance between the cells of origin and cancer stem cells in the Drosophila larval brain. Semin. Cell Dev. Biol. 28: 63–69

Jensen KB & Watt FM (2006) Single-cell expression profiling of human epidermal stem and transit-amplifying cells: Lrig1 is a regulator of stem cell quiescence. Proc. Natl. Acad. Sci. 103: 11958–11963

Jiang H-S, Wu Y-C (2014) LIN-3/EGF Promotes the Programmed Cell Death of Specific Cells in Caenorhabditis elegans by Transcriptional Activation of the Pro-apoptotic Gene egl-1. PLoS Genet 10(8): e1004513.

Joti, P., Ghosh-Roy, A. & Ray, K. (2011) Dynein light chain 1 functions in somatic cyst cells regulate spermatogonial divisions in Drosophila. Sci. Rep. 1, 173.

Kawasaki S, Tanioka H, Yamasaki K, Connon CJ & Kinoshita S (2006) Expression and tissue distribution of p63 isoforms in human ocular surface epithelia. Exp. Eye Res. 82: 293–299

Kiger AA, White-Cooper H & Fuller MT (2000) Somatic support cells restrict germline stem cell self-renewal and promote differentiation. Nature 407: 750–4

Kim K, Wu HG & Jeon SR (2015) Epidermal growth factor-induced cell death and radiosensitization in epidermal growth factor receptor-overexpressing cancer cell lines. Anticancer Res. 35: 245–254

Lajtha LG (1979) Stem Cell Concepts. Differentiation 14: 23–33

Lehrer MS, Sun TT & Lavker RM (1998) Strategies of epithelial repair: modulation of stem cell and transit amplifying cell proliferation. J. Cell Sci. 111, 2867-2875

Lenhart KF & DiNardo S (2015) Somatic Cell Encystment Promotes Abscission in Germline Stem Cells following a Regulated Block in Cytokinesis. Dev. Cell 34: 192–205

Levkoff LH, Marshall GP, Ross HH, Caldeira M, Reynolds BA, Cakiroglu M, Mariani CL, Streit WJ & Laywell ED (2008) Bromodeoxyuridine Inhibits Cancer Cell Proliferation In Vitro and In Vivo. Neoplasia 10: 804–IN13

Levin AJ (1997) p53, the Cellular Gatekeeper for Growth and Division. Cell, Vol. 88, 323–331

Li S, Wang H & Groth C (2014) Drosophila neuroblasts as a new model for the study of stem cell self-renewal and tumour formation. Biosci. Rep. 34(4), art:e00125

Li Y, Minor NT, Park JK, McKearin DM & Maines JZ (2009) Bam and Bgcn antagonize Nanos-dependent germ-line stem cell maintenance. Proc. Natl. Acad. Sci. 106: 9304–9

Luo L (2007) Fly MARCM and mouse MADM: Genetic methods of labeling and manipulating single neurons. Brain Res. Rev. 55: 220–227

Mandal L, Martinez-Agosto JA, Evans CJ, Hartenstein V & Banerjee U (2007) A Hedgehog- and Antennapedia-dependent niche maintains Drosophila haematopoietic precursors. Nature 446: 320–324

Mckearin DM & Spradling AC (1990) hag-of-marbles : a Drosophila gene required to initiate both male and female gametogenesis. Genes Dev.: 2242–2251

McLean PF & Cooley L (2013) Protein equilibration through somatic ring canals in Drosophila. Science (80). 340: 1444–1447

Monk A.C., Siddall N.A., Volk T., Fraser B., Quinn L.M., McLaughlin E.A. & Hime G.R. (2010) HOW is required for stem cell maintenance in the Drosophila testis and for the onset of transit-amplifying divisions. Cell Stem Cell, 6, pp. 348-360

Napoletano F, Gibert B, Yacobi-Sharon K, Vincent S, Favrot C, Mehlen P, Girard V, Teil M, Chatelain G, Walter L, Arama E & Mollereau B (2017) P53-Dependent Programmed Necrosis Controls Germ Cell Homeostasis During Spermatogenesis. PLoS Genet. 13: 1–21

Nurse P (1990) Universal control mechanism regulating onset of M-phase. Nature 344: 503–508

Ojeh N, Pastar I, Tomic-Canic M & Stojadinovic O (2015) Stem cells in skin regeneration, wound healing, and their clinical applications. Int. J. Mol. Sci. 16: 25476–25501

Papagiannouli F, Berry CW, Fuller MT (2018) The Dlg-module and clathrin-mediated endocytosis regulate EGFR signaling and cyst cell-germline coordination in the. bioRxiv: doi.org/10.1101/419937 [PREPRINT]

Parrott BB, Hudson A, Brady R & Schulz C (2012) Control of Germline stem cell division frequency - A novel, developmentally regulated role for Epidermal Growth Factor signaling. PLoS One 7(5): e36460.

Potten CS & Loeffler M (1990) Stem cells: attributes, cycles, spirals, pitfalls and uncertainties. Lessons for and from the crypt. Development 110: 1001–1020

Rangel-huerta E & Maldonado E (2017) Transit-Amplifying Cells in the Fast Lane from Stem Cells towards Differentiation. Stem Cells Int., vol. 2017, Article ID 7602951, 1-10

Reich A, Sapir A & Shilo B (1999) Sprouty inhibits RTK signaling. Development 126: 4139–4147

Rodgers JT, King KY, Brett JO, Cromie MJ, Charville GW, Maguire KK, Brunson C, Mastey N, Liu L, Tsai CR, Goodell MA & Rando TA (2014) MTORC1 controls the adaptive transition of quiescent stem cells from G0to GAlert. Nature 510: 393–396

Roth TM, Chiang C-YA, Inaba M, Yuan H, Salzmann V, Roth CE & Yamashita YM (2012) Centrosome misorientation mediates slowing of the cell cycle under limited nutrient conditions in Drosophila male germline stem cells. Mol. Biol. Cell 23: 1524–1532

Seidel HS & Kimble J (2015) Cell-cycle quiescence maintains Caenorhabditis elegans germline stem cells independent of GLP-1/Notch. Elife 4: 1–28

Sheng XR & Matunis E (2011) Live imaging of the Drosophila spermatogonial stem cell niche reveals novel mechanisms regulating germline stem cell output. Dev. Stem Cells 138: 3367–3376

Sigrist S, Ried G & Lehner CF (1995) Dmcdc2 kinase is required for both meiotic divisions during *Drosophila* spermatogenesis and is activated by the Twine/cdc25 phosphatase. Mech. Dev. 53: 247–260

Taupin P (2007) BrdU immunohistochemistry for studying adult neurogenesis: Paradigms, pitfalls, limitations, and validation. Brain Res. Rev. 53: 198–214

Treda C, Popeda M, Ksiazkiewicz M, Grzela DP, Walczak MP, Banaszczyk M, Peciak J, Stoczynska-Fidelus E & Rieske P (2016) EGFR Activation Leads to Cell Death Independent of PI3K/AKT/mTOR in an AD293 Cell Line. PLoS One 11: 1–17

Wang C, Guo X & Xi R (2014) EGFR and Notch signaling respectively regulate proliferative activity and multiple cell lineage differentiation of Drosophila gastric stem cells. Nat. Publ. Gr. 24:

Weng M, Golden KL & Lee C-Y (2010) dFezf/Earmuff Maintains the Restricted Developmental Potential of Intermediate Neural Progenitors in Drosophila. Dev. Cell 18: 126–135

Wylie A, Lu WJ, D'Brot A, Buszczak M & Abrams JM (2014) p53 activity is selectively licensed in the Drosophila stem cell compartment. Elife 2014:

Xie T, Spradling AC, Potten CS, Loeffler M, Morrison SJ, Shah NM, Anderson DJ, Watt FM, Hogan BLM, Shamblott MJ, Brustle O, Weissman IL, Spradling A, Lin H, Cuevas M de,

Spradling A, Deng W, Lin H, Margolis J, Spradling A, et al (2000) A niche maintaining germ line stem cells in the Drosophila ovary. Science 290: 328–30

Yang H & Yamashita YM (2015) The regulated elimination of transit-amplifying cells preserves tissue homeostasis during protein starvation in Drosophila testis. Development 142: 1756–1766

Zhang B & Hsu YC (2017) Emerging roles of transit-amplifying cells in tissue regeneration and cancer. Wiley Interdiscip. Rev. Dev. Biol. 6: 1–14

Zhao R, Xuan Y, Li X & Xi R (2008) Age-related changes of germline stem cell activity, niche signaling activity and egg production in Drosophila. Aging Cell 7: 344–354

Zielke N, Korzelius J, Straaten M Van, Bender K, Schuhknecht GFP, Dutta D, Xiang J & Edgar BA (2014) Resource Fly-FUCCI : A Versatile Tool for Studying Cell Proliferation in Complex Tissues. Cell Reports 7: 588–598

Figure legends:

Figure 1: Stage-wise distribution of germline cysts and that of the cell cycle phases during the TA.

A) Schematic illustrates the process of transit amplification during early spermatogenesis and expressions domains of the germ cell markers, nanos (nos) and bag-of-marbles (bam), and a somatic cell marker traffic-jam *in Drosophila*. Glossary: GSC – Germline Stem Cell, CySC – Cyst Stem cell, SSC – Somatic Cyst Cell, GB – Gonialblast, SG – Spermatogonia.
B) The apical tip of wild-type (WT) testis stained with the Hoechst-dye (blue), anti-Armadillo (Red) and anti-Vasa (green). GSC, GB, 2-cell, and 16-cells are indicated by arrows, and the scale bar indicates ~ 20μm.
C) Enlarged images of the hub, GSCs, and cysts at different stages of TA in wild-type testis.
D) Stage-wise distribution of average (± S.E.M) germline cysts (grey bars) and cysts stained with various cell cycle markers (average ± S.E.M.) in the WT background. The pair-wise significance of difference was estimated using the Mann-Whitney-U test, and the p-values and sample numbers are indicated on the plot.
E) WT testes stained with vasa (Red) and different cell cycle markers (green) indicate the distribution of cell cycle phases in the germline of cysts at different stages. Although it marked very few cysts in testis, the CycE (a), CycA (c), and PH3 (e) immunostaining and the expressions of ΔPCNA-GFP (b) and GFP-CycB protein trap (d) always marked all the germline cells within the cyst. Scale bars indicate ~20μm.

Figure 2: Stage-wise distribution of cysts in the background of early germline-specific RNAi of *cdc25/string* (stg), *CDK1* and overexpression of Dp53

A-D) Testes from *nos>EGFP* (A), *nos>stg*^{dsRNA} (B), *nos>Cdk1*^{dsRNA} (C) and *nos>dp53* (D) flies, stained with the Hoechst dye (blue), anti-Arm (Red), Lysotracker (red) and anti-Vasa (green), show shrunken apical tip with fewer cysts as compared to control (A) (scale bars ~20μm).
E) The histograms depict the stage-wise distribution (average ± S.D.) of cysts (E) in the *stg* and *Cdk1* RNAi and dp53 overexpression backgrounds.
F) The histograms depict the stage-wise distribution (averages) of phospho-histone3 positive cysts in the *stg* and *Cdk1* RNAi and dp53 overexpression backgrounds.

The pair-wise significance of difference was estimated using the Mann-Whitney-U test (p-values are * <0.05, **<0.01, ***<0.001) and the sample numbers are as indicated on the histogram panels.

Figure 3: Stage-wise distribution of cysts in the background of late germline-specific RNAi of *cdc25/string* (*stg*) and *Cdk1*

A) (a)Testes from *bam>stg*^{dsRNA} (a), stained with the Hoechst dye (blue), anti-Arm (Red), Lysotracker (red) and anti-Vasa (green), (scale bars ~20μm). (b) The histograms depict the stage-wise distribution (average ± S.D.) of cysts in the *stg* RNAi.
B) Testes from *bam>Cdk1*^{dsRNA} (a, b), stained with the Hoechst dye (blue), anti-Arm (Red), Lysotracker (red) and anti-Vasa (green), (a) The dotted line demarcates the early stages (GSC to 4-cell stages). (Scale bars ~20μm). (b) The dotted line demarcates the early

stages (GSC to 4-cell stages), and the arrows mark a few of the 8-cell cyst. (Scale bars ~100μm). (c) The histograms depict the stage-wise distribution (average ± S.D.) of cysts (b) in the *Cdk1* RNAi background.

The pair-wise significance of difference was estimated using the Mann-Whitney-U test (p-values are * <0.05, **<0.01, ***<0.001) and the sample numbers are as indicated on the histogram panels.

Figure 4: Alteration in the stage-wise distribution of cysts and germ cell death with a progressive increase in the EGFR signaling in SCCs during the TA stages.

A) The schematic depicts the EGFR signaling in the germline. (SCC- Somatic Cyst cell)
B) Experimental paradigm for temperature regulated overexpression.
C) Histograms represent the average (±S.D.) germline cells, and the line plot depicts the number of GSCs (average ± S.D.) in the control (*tjGal4; tubGal80^{ts}>UAS-mCD8RFP*) (a), and conditional *EGFR^{CA}* (*tjGal4; tubGal80^{ts}>UAS-EGFR^{CA}*) overexpression (b) backgrounds after different durations of growth under the non-permissive condition (illustrated by the schematics). The sample numbers (n) are as indicated at the bottom of the histogram panels.
D) Stage-wise cyst distribution (average ± S.D.) in the control (grey bars) and *EGFR^{CA}* overexpression backgrounds at 0 hour and after 96 hours of growth under the non-permissive condition. The sample numbers are as indicated on the histogram panels.
E) (a) Histograms depict the average lysotracker-positive cysts in the control (*tjGal4; tubGal80^{ts}>UAS-mCD8RFP)* (grey bars) and EGFR^{CA} overexpression (*tjGal4; tubGal80^{ts}>UAS-EGFR^{CA}*) (red bars) backgrounds at different durations of growth at 30°C.
(b) The lysotracker-positive cysts in the spermatocyte region (identified by the appearance of round morphology and enlarged size shown in S2 C,D) increased significantly after 24 hours.

The pair-wise significance of difference was estimated using the Mann-Whitney-U test. (p-values are * <0.05, **<0.01, ***<0.001)

Figure 5: Upregulation of EGFR signaling by overexpression of ligand in the germline and their effects on the cyst distribution profile.

A) The apical part of a *nos>sSpi-GFP* testis indicating the expression of *sSpi-GFP* (green in a, and FIRE LUT in b) in GSCs and GBs (arrowhead in b) around the hub (*). Germ cells are marked by the Vasa staining (magenta in a). The expression of *UAS-EGFP* (FIRE LUT) in *nos>EGFP* (c) labeled germline cells in all TA stage cysts with progressively reduced intensity, and in *bam>EGFP* (d) labeled the germline from the 4-cell stage (arrow).
B) (a) Apical parts of adult testes from the *nos>sSpi-GFP* overexpression background stained with the Hoechst dye (Blue), anti-Vasa (green) and anti-Arm (red) (scale bar ~10μm).
(b) Histograms depict stage-wise cyst distributions (average ±S.D.) in the *nos>EGFP* control and *nos>sSpi-GFP* overexpression backgrounds.
C) The stage-wise cyst distributions of average PH3-positive cysts in the control and *sSpi-GFP* overexpression backgrounds.
D) a) A *bam>sSpi-GFP* testis stained with the Hoechst dye (Blue), anti-Vasa (green) and anti-Arm (red) and lysotracker (red) (scale bar ~20μm). (b) Histograms depict stage-wise

cyst distributions (average ±S.D.) in the *bam>EGFP* (control) and *bam>sSpi-GFP* backgrounds.

The pair-wise significance of difference was estimated using the Mann-Whitney-U test (p-values are * <0.05, **<0.01, ***<0.001) and the sample numbers are as indicated on the histogram panels.

Figure 6: Upregulation of EGFR signaling by knockdown of negative feedback in the somatic cells and their effects on the cyst distribution profile.

A) The schematic illustrates the role of downstream feedback regulators – argos (aos) and kekkon (kek)- in moderating the EGFR signaling at three distinct levels (adapted from Shilo, 2005).

B, C) The patterns of *aos-GFP*^{fosmid} (A) and *kek1-GFP* enhancer trap (B) expressions in the wild-type

D, F, H) Apical parts of adult testes from the tjGal4 driven *aos* (D), *kek2* (F) and *kek1* (H) RNAi backgrounds stained with the Hoechst dye (Blue), anti-Vasa (green) and anti-Arm (red) (scale bars ~20μm).

E, G, I) Histograms show the cyst distribution (average ± S.D.) in the *tjGal4* (control), and in the *aos*, *kek2* and *kek1* RNAi backgrounds.

J) Histograms describe stage-wise distribution of average PH3-positive cysts in the control, and in the *aos, kek2* and *kek1* RNAi backgrounds.

The pair-wise significance of difference was estimated using the Mann-Whitney-U test (p-values are * <0.05, **<0.01, ***<0.001) and the sample numbers are as indicated on the histogram panels.

Table 1: Estimated persistence time of different cyst stages during the TA in different genetic backgrounds.

Genotype	T0 (GSC)	T1 (GB)	T2 (2-cell)	T3 (4-cell)	T4 (8-cell)
	Hours				
Wild Type (Canton-S) (25°C)	26.8	30.8	29.8	13.1	11.1
***nos* (control)**	14.8	29	23.3	12.8	9.7
***tj* (control)**	19.6	19.1	15.4	6.9	5.6

Table 2: Estimated persistence time of different cyst stages during the TA in different germline cell cycle perturbation backgrounds.

Genotype	T0 (GSC)	T1 (GB)	T2 (2-cell)	T3 (4-cell)	T4 (8-cell)
	Hours				
***nos* (control)**	14.8	29	23.3	12.8	9.7
nos>stg^{dsRNA}	23.3	22.7	27.5	11	7.6
nos>Cdk1^{dsRNA}	26.1	27.5	30.9	11.5	11.9
nos>dp53	107.9	151.5	135.8	47	47

Table 3: Estimated persistence time of different cyst stages during the TA in germline driven secretory Spitz overexpression backgrounds.

Genotype	T0 (GSC)	T1 (GB)	T2 (2-cell)	T3 (4-cell)	T4 (8-cell)
	Hours				
***nos* (control)**	14.8	29	23.3	12.8	9.7
nos>sSpi-GFP	31.4	37.9	53.9	32.5	29.5

Table 4: Estimated persistence time of different cyst stages during the TA in different negative feedback knockdown backgrounds.

Genotype	T0 (GSC)	T1 (GB)	T2 (2-cell)	T3 (4-cell)	T4 (8-cell)
	Hours				
***tj* (control)**	19.6	19.1	15.4	6.9	5.6
tj>aos^{dsRNA}	38.7	32.3	35.9	20.2	15.1
tj>kek2^{dsRNA}	44.4	39.2	40.3	25.4	30.5

Figure 1: Stage-wise distribution of germline cysts and that of the cell cycle phases during the TA.

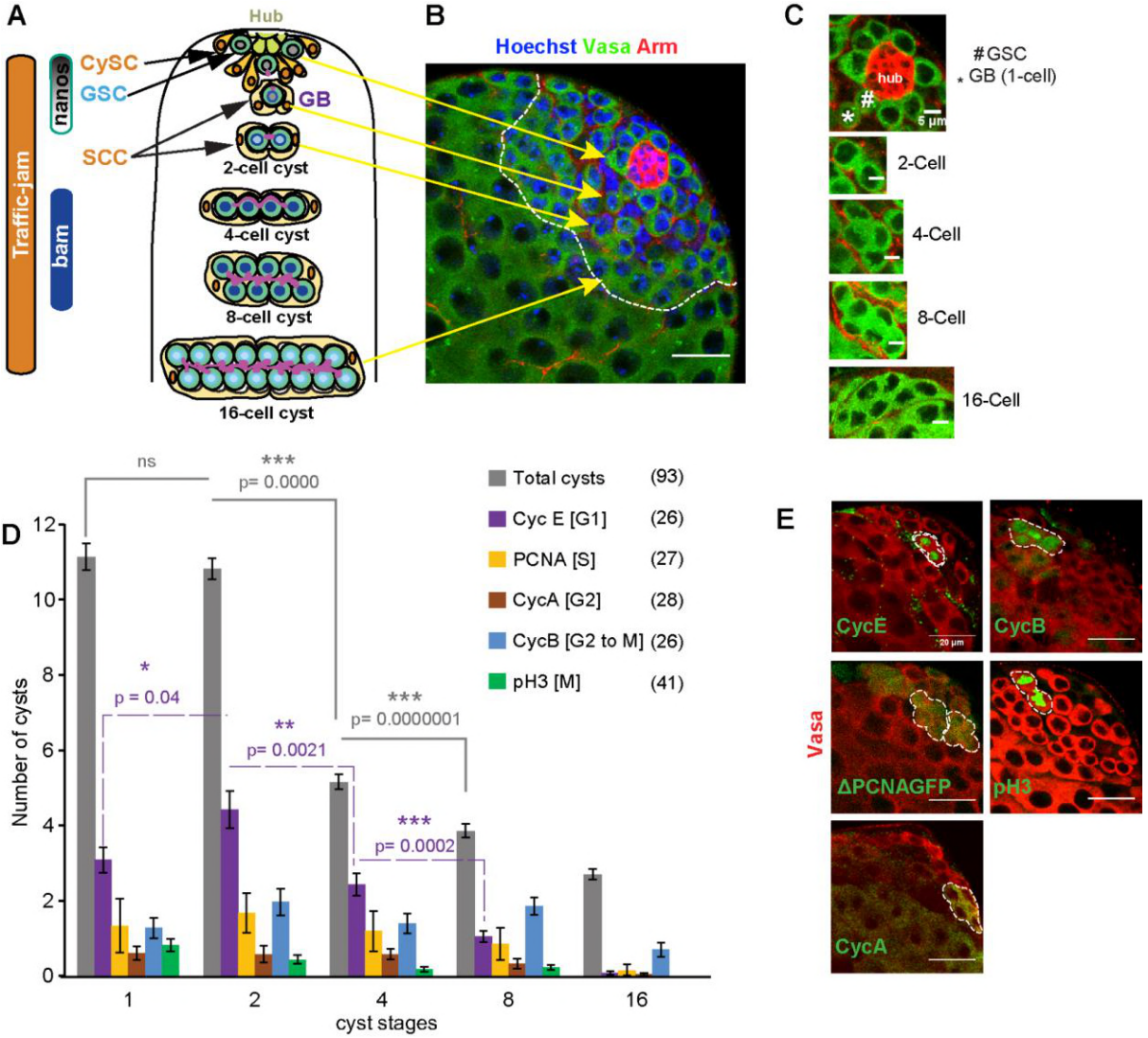

Figure 2: Stage-wise distribution of cysts in the background of early germline-specific RNAi of *cdc25/string* (stg), *CDK1* and overexpression of Dp53

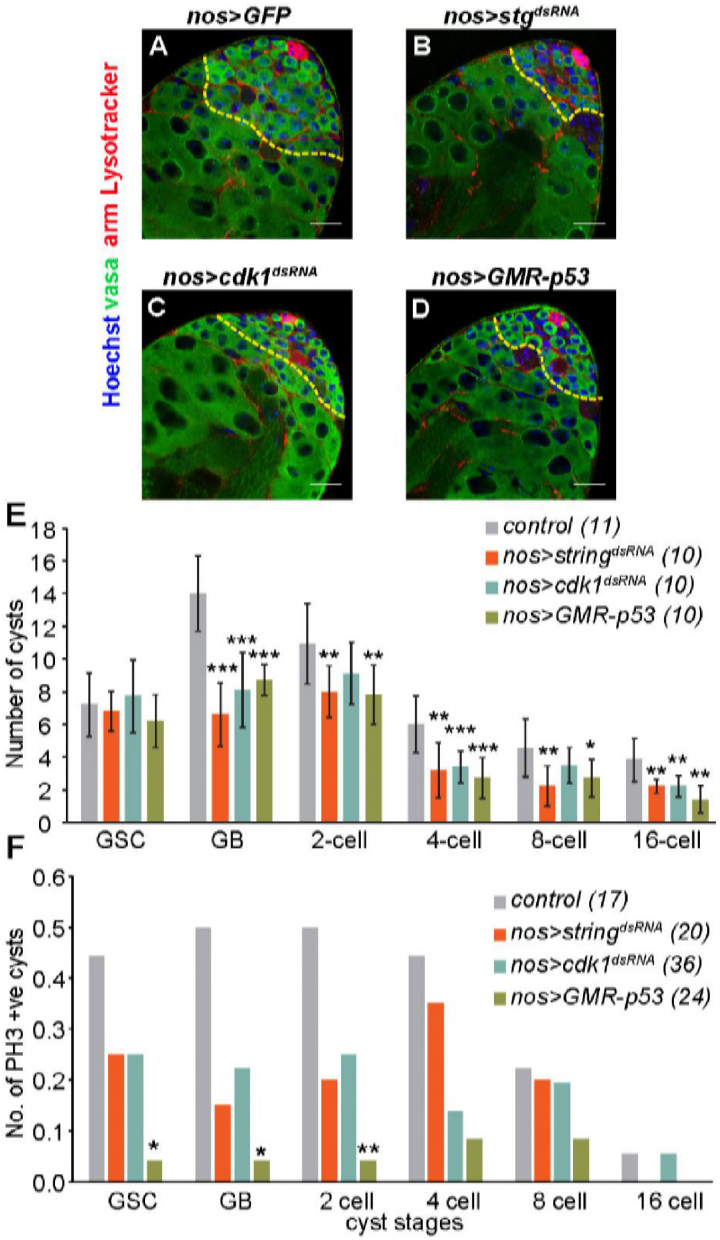

Figure 3: Stage-wise distribution of cysts in the background of late germline-specific RNAi of cdc25/string (stg) and Cdk1

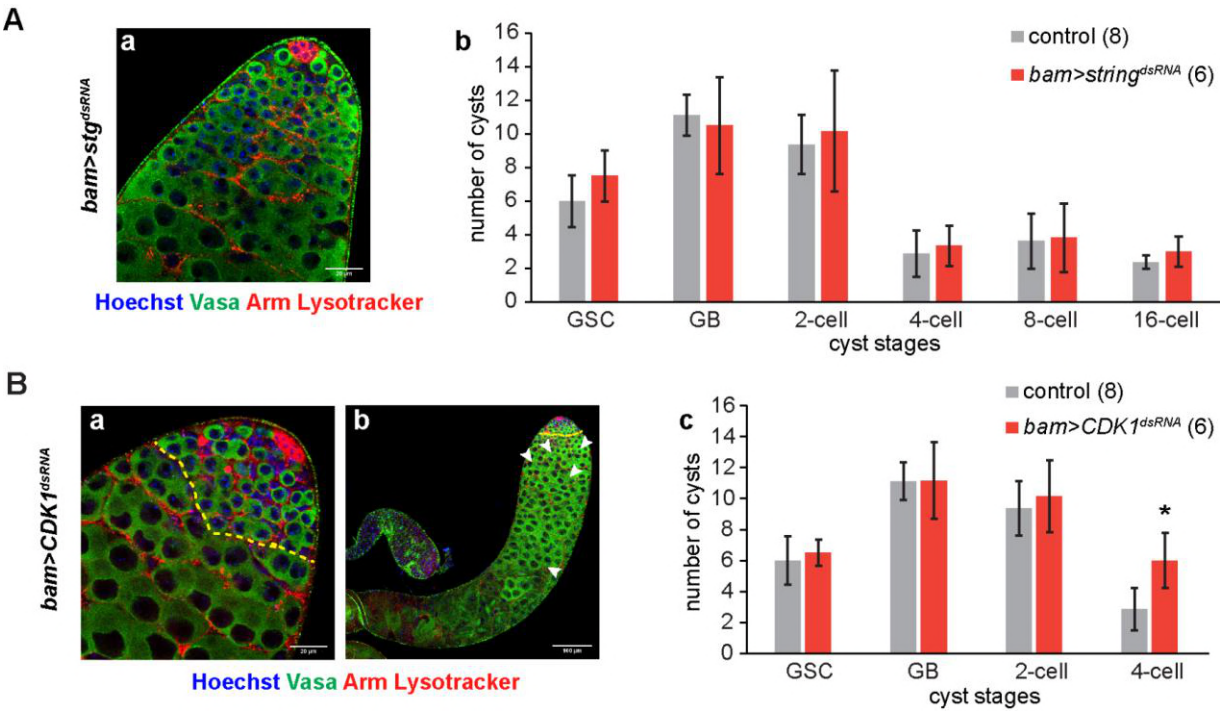

Figure 4: Alteration in the stage-wise distribution of cysts and germ cell death with a progressive increase in the EGFR signaling in SCCs during the TA stages.

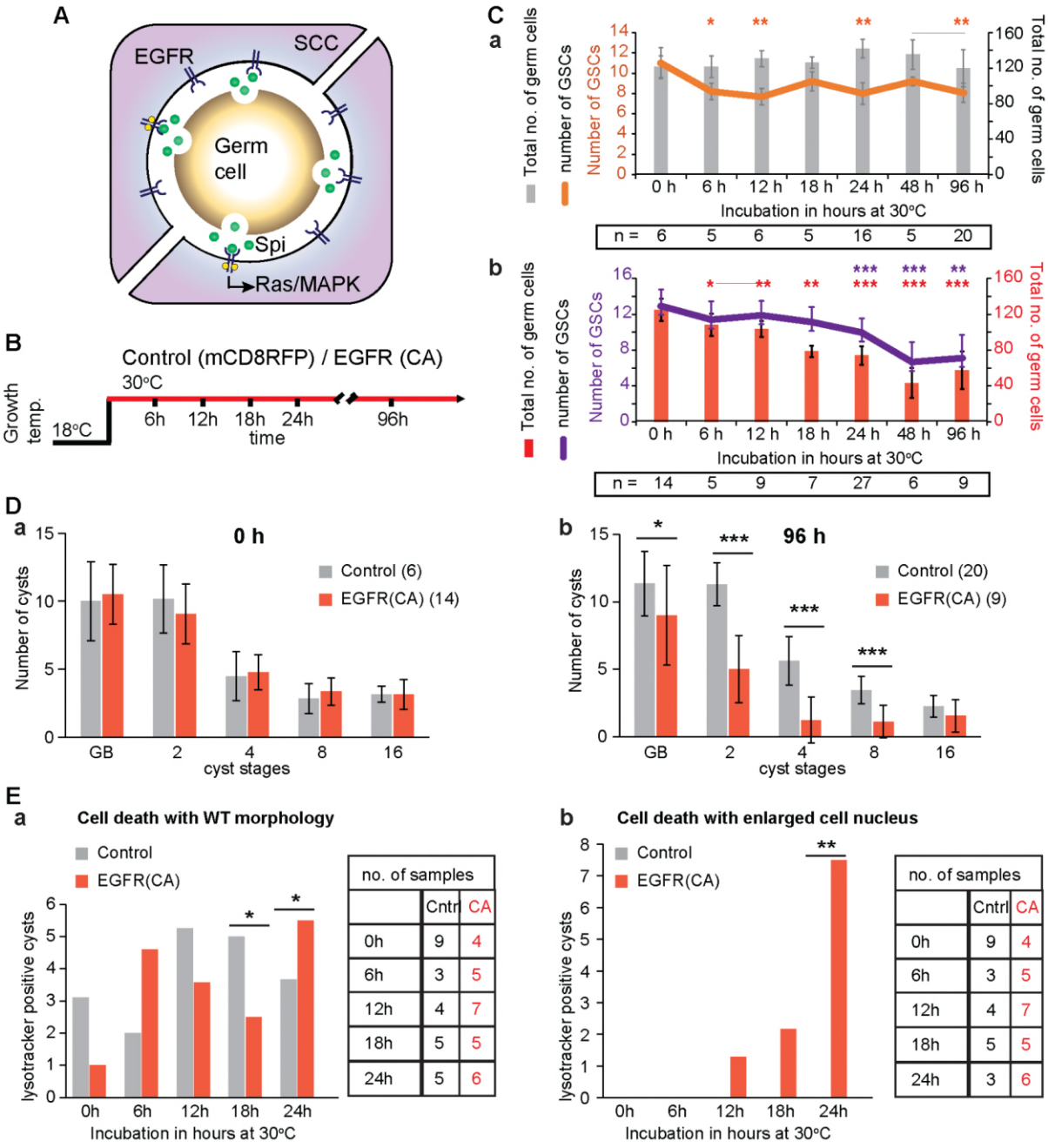

Figure 5: Upregulation of EGFR signalling by overexpression of ligand in the germline and their effects on the cyst distribution profile.

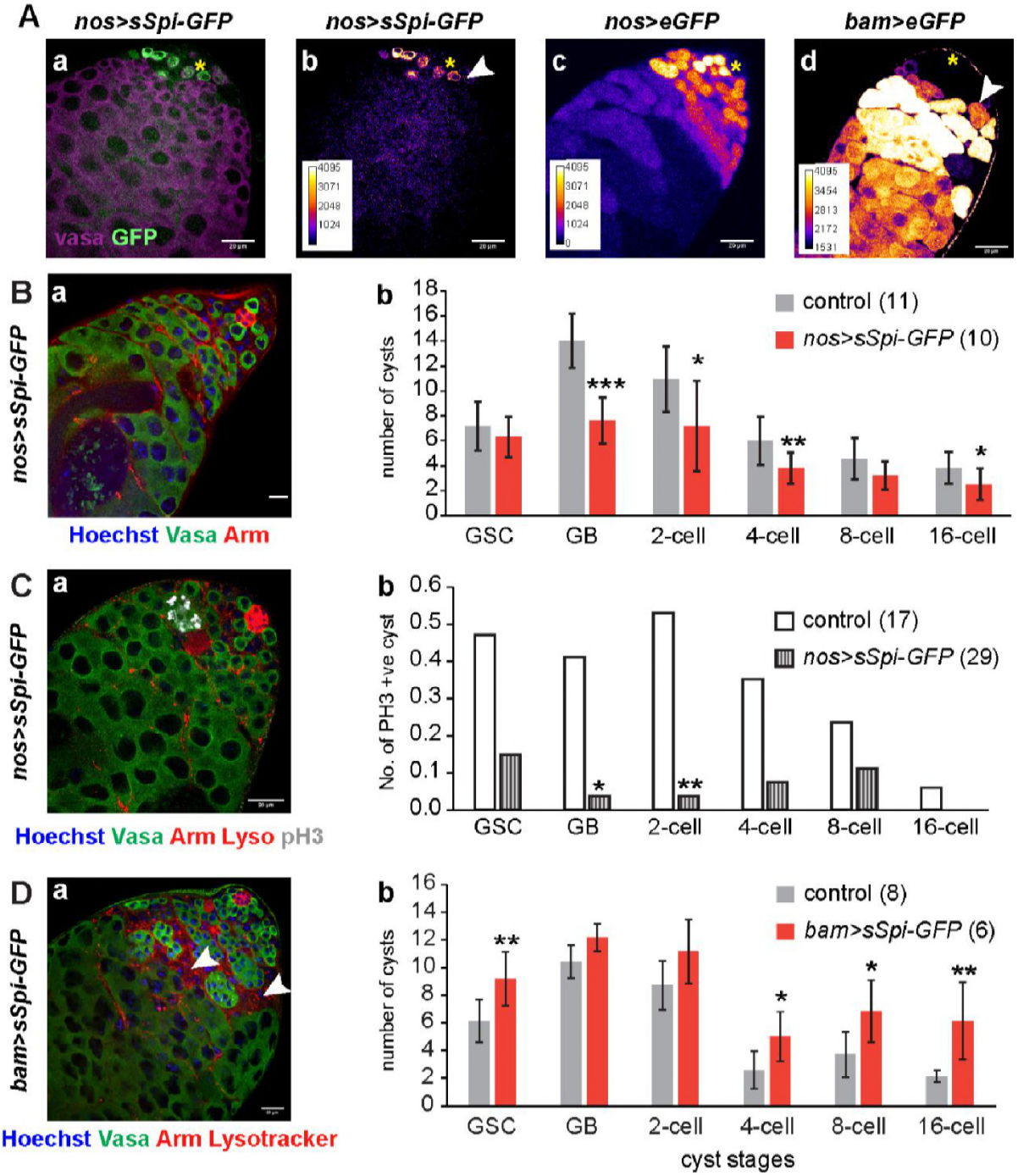

Figure 6: Upregulation of EGFR signalling by knockdown of negative feedback in the somatic cells and their effects on the cyst distribution profile